Journal Pre-proof

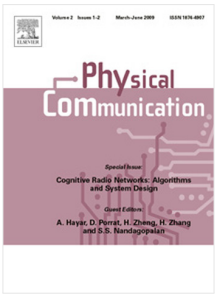

Unmanned aerial vehicles assisted rice seedling detection using shark smell optimization with deep learning model

Yousef Asiri

PII: S1874-4907(23)00082-4
DOI: https://doi.org/10.1016/j.phycom.2023.102079
Reference: PHYCOM 102079

To appear in: *Physical Communication*

Received date : 28 January 2023
Revised date : 29 March 2023
Accepted date : 9 April 2023

Please cite this article as: Y. Asiri, Unmanned aerial vehicles assisted rice seedling detection using shark smell optimization with deep learning model, *Physical Communication* (2023), doi: https://doi.org/10.1016/j.phycom.2023.102079.

Unmanned Aerial Vehicles Assisted Rice Seedling Detection using Shark Smell Optimization with Deep Learning Model

Yousef Asiri[1,*]

[1]Department of Computer Science, College of Computer Science and Information Systems, Science and Engineering Research Center, Najran University, Najran 61441, Saudi Arabia; yasiri@nu.edu.sa

Abstract

Rice seedling classification using an unmanned aerial vehicle (UAV) images remains a challenging problem that needs to be addressed. It is still a difficult task because it is prone to low temporal and spatial resolution images. Recently, machine learning (ML) and deep learning (DL) models can be employed for several image preprocessing tasks such as classification, object detection, and segmentation. Therefore, this study focuses on the design of shark smell optimization with deep learning based rice seedling detection (SSODL-RSD) on UAV imagery. The presented SSODL-RSD technique recognizes the UAV images into arable land and rice seedlings. To achieve this, the SSODL-RSD technique employs the adaptive Wiener filtering (AWF) technique for the noise removal procedure. In addition, the SSODL-RSD technique exploits the NestNet feature extractor model. Moreover, the SSO algorithm is used for the hyperparameter tuning of the NestNet model. Finally, the long short term memory-recurrent neural network (LSTM-RNN) model is employed for the classification of rice seedlings. The extensive comparative study highlighted the improved outcomes of the SSODL-RSD technique over other existing models.

Keywords: Unmanned aerial vehicles; Agriculture; Deep learning; Aerial robots; Shark smell optimization

1. Introduction

Recently, remote sensing images from unmanned aerial vehicles (UAV) imagery can be employed to enhance the performance and suitability of agricultural data [1]. Advanced open access satellites, like the Sentinel series functioned by the European Space Agency, offer a broader coverage area (100 km by 100 km image tiles) with the reexamining occurrence of some days; however, it is restricted to image resolution [2]. The UAV images assist remote sensing based crop analysis by the use of reference images with high resolution. They can be

employed to obtain data related to the crop types locally and produce ground truth datasets to train the UAV based approaches [3]. Due to the high resolution, crop classification finds useful for wide mono-cropped filed and also in small agricultural fields [4]. The need for farming products desires agriculture sectors to accommodate the latest technologies to resolve the challenging issues related to productivity [5]. Predominantly, populace development builds continuous pressure on the agricultural industry for an increased supply of foods to satisfy the global need, where the farmers need to utilize advanced technologies to improve crop productivity.

Generally, precision agriculture plays a vital role in increasing the quality of crop productivity, supporting crop productivity and making a decision depending upon a large quantity of data and details related to crop status attained in the farmlands [6]. Rice is an important grain used by people globally. For accurate prediction of the rice quality and yield [7], exploring rice seedlings is essential, which is an important factor in examining uniform maturity and cultivation density of precision farming [8]. To achieve this, deep learning (DL), which is a field of machine learning (ML), has been employed for detecting objects in high-density scenes with complex backgrounds. With the training of a massive quantity of image data, object recognition can precisely recognize the target objects and the spatial positions in the images, categorize objects from the quantified changes and mask the objects in the bounding boxes via effective models [9]. Available object detectors can recognize big or small-sized objects in the more significant parts of the image. In addition, the critical problem in computer vision (CV) lies in detecting the smaller objects from the imagery, which lack presence data in differentiating them from the backdrop and identical classes [10].

This study focuses on the design of shark smell optimization with deep learning based rice seedling detection (SSODL-RSD) on UAV imagery. The SSODL-RSD technique recognizes the UAV images in arable land and rice seedlings. To accomplish this, the SSODL-RSD method employs the adaptive Wiener filtering (AWF) technique for the noise removal procedure. In addition, the SSODL-RSD method exploits the NestNet feature extractor model. Moreover, the SSO algorithm is used for the hyperparameter tuning of the NestNet model. Finally, the long short term memory-recurrent neural network (LSTM-RNN) approach was employed for the classification of rice seedlings. The experimental evaluation of the SSODL-RSD technique is tested on a rice seedling dataset.

2. Related Works

In [11], the authors intended to discover many deep CNN (DCNN) techniques for determining that one accomplishes the optimum for defective paddy seedling recognition utilizing aerial images. Therefore, the authors estimated the robustness, accuracy, and inference latency of one- and two-step pre-training object detector integrated with recent extracting features like MobilenetV2, EfficientNet, and ResNet50 as the backbone. The authors also examined the outcome of transfer learning (TL) by fine-tuning the efficiency of the above-mentioned pre-trained approaches. Tseng et al. [12] purpose of this analysis is to detect rice seedlings from rice fields utilizing TL in 2 ML approaches, Faster R-CNN and EfficientDet-D0, and related to the outcomes of the legacy system—HOG based SVM classifier. This analysis depends on a crucial UAV image database for building a method for detecting tiny rice seedlings. Yang et al. [13] examine a semi-auto annotation system with an ExGR index for generating the trained data of paddy seedlings. To demonstrate, this investigates improved a typical CNN infrastructure, VGG16, to run a patch-based rice seedling recognition.

Wu et al. [14] present an effectual approach which utilizes CV to correctly amount paddy seedlings from digital imagery. Primarily, a UAV equipped with RGB cameras is employed for acquiring domain images at the seedling stage. Afterwards, the authors utilize a regression network (Basic Network) simulated by deep fully CNN for regressing the density map and evaluation of the rice seedlings count to provide UAV imagery. Wang et al. [15] presented a new and quick paddy seedling row detection system dependent upon a row vector grid classifier. This approach creates an end-to-end CNN technique collected of seedling extracted features and row vector grid classifier that changes seedling row detection as to grid classifier problem dependent upon row vector utilizing the global feature.

In [16], the author is primarily present for utilizing HOG descriptor for characterizing paddy seedling imagery. While the image size is entirely arbitrary, the extracting feature by HOG could not be utilized directly by classification because of the distinct dimensional. The authors execute many imputation systems for filling the absence of data for the HOG descriptor. In [17], RGB colour images of seedlings paddy are taken in rice fields, and ground truth (GT) images can be attained by automatically labelling the pixel from the RGB imagery with three distinct types of weed, rice seedlings, and background. The class weighted coefficients can be estimated for resolving the unbalance problem of the count of classifier types. GT and RGB images can be utilized for training and testing data. The presented methodology can be related to a typical semantic segmentation system such as U-Net and FCN techniques.

3. The Proposed Model

In this study, we have concentrated on developing the SSODL-RSD technique for rice seedling classification on UAV imagery. The presented SSODL-RSD procedure encompasses AWF based image enhancement, NestNet feature extraction, SSO based hyperparameter tuning, and LSTM-RNN based classification. Fig. 1 represents the block diagram of the SSODL-RSD approach.

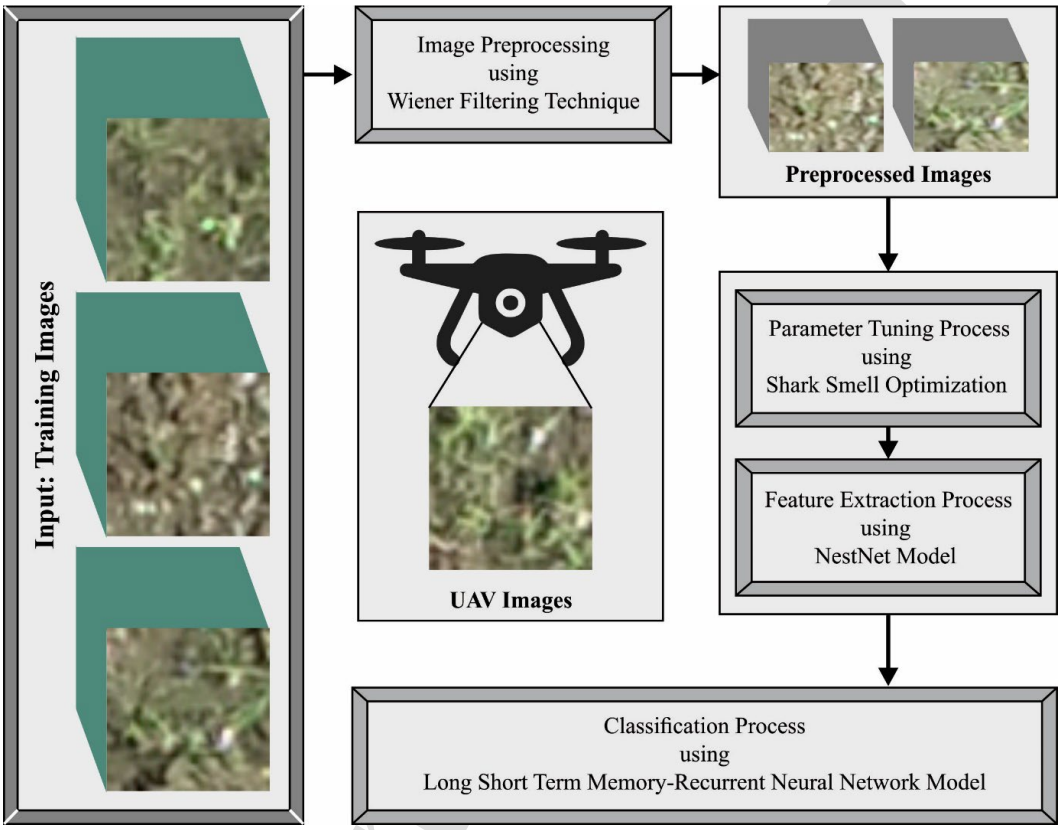

Fig. 1. Block diagram of SSODL-RSD approach

3.1. AWF based Preprocessing

At the introductory level, the SSODL-RSD technique employed the AWF technique for the noise removal procedure. The AWF technique eradicates the nodes and helps to investigate the place of contours accurately [18]. It effectually preserves the image edges and decreases the noise level via the filters. The regional mean and variance can be examined by substituting the gray levels. The regional mean can be defined using Eq. (1):

$$b = \frac{1}{CD} \sum_{k_1,k_2 \in K} G\,(k_1, k_2) \tag{1}$$

where C and D denote window length and width, K designates the input image value chosen in window size, k_1, k_2 indicate the coordinate points of the input image selected via the window size, and G represents the input image. The variance can be defined as follows.

$$\sigma^2 = \frac{1}{CD} \sum_{k_1,k_2 \in K} G^2\,(k_1, k_2) - b^2 \tag{2}$$

Where b defines the regional average. The coordinate points can be denoted as follows.

$$f(k_1, k_2) = b + \frac{\sigma^2 - q^2}{\sigma^2}(G(k_1, k_2) - b) \tag{3}$$

where q^2 is noise variance.

3.2. NestNet based Feature Extraction

Here, the SSODL-RSD technique exploited the NestNet feature extractor model. The NestNet approach incorporates a pair of parallel modules for processing images at varying time intervals [19]. The NestNet approach comprises two portions, namely the encoding unit and the decoding unit. The encoding unit produces feature vectors, and it has four hierarchical ranks. A rise in channel count leads to high computation complexity in deriving image features. The parallel processing blocks in the NestNet approach can eliminate it. The next decoding unit fuses the feature data and performs feature upsampling to the image of identical width and height.

The encoding unit involves the extraction of multi-scale convolution features from images X and Y. In addition, $F_{X|Y}^{i,j}$ denotes the features from image X or Y, $F_{X|Y}^{i,j}$ can be computed as follows.

$$F_{X|Y}^{i,j} = c(\emptyset\left(F_{X|Y}^{i,j-1}, u\left(F_{X|Y}^{i+1,j-1}\right)\right) \tag{4}$$

$$s.t.\, i, j \in \{(0,1), (0,2), (1,1), (2,1)\}$$

And

$$F_{X|Y}^{i,j} = d\left(F_{X|Y}^{i-1,j}\right) \tag{5}$$

$$\text{s. t. i, } j \in \{(1,0),(2,0),(3,0),(4,0)\}$$

Where $F_{X|Y}^{i,j}$ and $F_{X|Y}^{i,j}$ denotes feature vectors from image X or Y, $c(\cdot)$ represents the Concat function which combines the features via channels, u signifies upsampling process, which upsamples the width and height of the features, d means a downsampling function which downsamples the width and height of the feature to 1/2 of the actual size. $\emptyset$ symbolizes the computation of the encoding module, and X|Y denotes X or Y.

The ADO was applied for fusing the features and can be formulated as follows.

$$F_D^i = \sigma\left(F_x^{a,b}, F_Y^{a,b}\right) \tag{6}$$

$$s.t.\, i \in 1, \ldots 9$$

where $F_x^{a,b}$ and $F_Y^{a,b}$ indicate. The result of the initial element $(D^1 - D^9)$ can be treated as the input of the decoding unit where the features of the similar level are skip connected to other features. We employ $F_{X,Y}^{i,j}$ to depict $XY^{i,j}$, where $F_{X,Y}^{i,j}$ can be defined below.

$$F_{X,Y}^{i,j} = c\left(u\left(F_{X,Y}^{a,b}\right), F_D^t, \emptyset\left(F_{X,Y}^{c,d}\right)\right) \tag{7}$$

where $F_{X,Y}^{a,b}$ and F_D^t indicate the values of $XY^{a,b}$ and D^t. The output data O^1, $O2, O^3$, O^4 and O^5 can be represented as follows.

$$F_o^i = \emptyset(F_D^{i-1}) s.t.\, i \in 1,2$$

$$F_o^j = \emptyset(F_{X,Y}^{0,j})\ s.t.\, j\ \in 3,4 \tag{8}$$

$$F_o^5 = \emptyset\left(c(F_o^1, F_o^2, F_o^3, F_o^4)\right) \tag{9}$$

Where F_o^i denotes the value of O^i. The dense block can be employed at the top three layers of the decoding unit to enhance the performance of the feature utilization process.

3.3. SSO based Hyperparameter Tuning

Next to feature extraction, the SSO algorithm is used for the hyperparameter tuning of the NestNet model. The shark widely applies their strong smell sense to catch the prey [20]. The shark odour concentration is the most effective sense. Subsequently, the shark has the capacity to sense an injured fish from 1km away. The shark odour concentration deliberated as a guide

for it. This process might assist to find the odour source. In the present proposal, concentration perform a key role in guiding the shark to its prey. On the other hand, higher odour outcomes in the precise movement of the shark. These features are the base for the proposal of an optimization method to find an ideal solution. The search procedure begins once the shark senses the odour intensity. In fact, the odour particles contain weaker diffusion from the damaged fish (prey). For modelling these processes, a population of initial solutions is randomly produced for optimizing the problem from the potential searching range. All the solutions represent the odour particles which illustrates the potential position of the shark at the first search method. Fig. 2 represents the steps involved in the SSO technique.

$$[x_1^1, x_2^1, \dots, x_{\mathrm{NP}}^1] \tag{10}$$

Whereas $x_i^1 = i^{th}$ solution or i^{th} initial position of population vector, and NP indicates the population size, and it can be expressed as follows:

$$x_i^1 = \left[x_{\mathrm{i},1}^1, x_{\mathrm{i},2}^1, \dots, x_{\mathrm{i,NP}}^1\right] i = 1,2, \dots, NP, \tag{11}$$

Where $x_{i,j}^1 = j^{th}$ dimension of shark i^{th} location or j^{th} decision parameter of the ith location of shark (x_i^1); and $ND =$ amount of decision variable in optimization problems. The smell intensity at all the locations reflects the closeness to the prey. The shark at all locations travels with the velocity approach to the prey. Based on the location vector, the primary velocity vector is provided as follows:

$$[V_1^1, V_2^1, \dots, V_{\mathrm{NP}}^1] \tag{12}$$

Now, the velocity vector has a set of components in all the dimensions.

$$V_i^1 = \left[V_{\mathrm{i},1}^1, V_{\mathrm{i},2}^1, \dots, V_{\mathrm{i,NP}}^1\right] i = 1, \dots, ND \tag{13}$$

The shark tracks the odour, and the course of the movement is intended based on the odour concentration. The shark velocity has raised due to the enhanced odour concentration. The gradient demonstrates the direction where the procedure increases with maximal rate, as given below:

$$V_i^k = \eta_k . R1 . \nabla(OF)|_{x_i^k} \; i = 1, \dots, NP \; k = 1, \dots, k_{max}, \tag{14}$$

Now, V_i^k indicates the velocity of the shark, OF shows the objective function, r represents the gradient of an objective function, $k_{\max}$ denotes the maximum amount of stages to forward

movement of the shark, k indicates the stage count, η_k = a value ranges within [0,1], and $R1$ shows the arbitrary number which follows uniform distribution within [0,1]. η_k shows a range from zero to one because it is not feasible for the shark to accomplish the velocity determined by the gradient function. The parameter $R1$ offers another arbitrary search intrinsic to the SSO approach. The velocity in all the dimensions is evaluated by:

$$V_{\mathrm{i},j}^{k} = \eta_k . R1 = \frac{\partial(\mathrm{OF})}{\partial x_j}|_{x_{ij}^{k}} . \mathrm{i} = 1, \dots, \mathrm{NP\ j} = 1, \dots, ND\ k = 1, \dots, k_{\max} \quad (15)$$

Due to the incidence of inertia, the acceleration of the shark is constrained, and the velocity depends on the previous velocity. This procedure is given as follows:

$$V_{\mathrm{i},j}^{k} = \eta_k . R1 . \frac{\partial(\mathrm{OF})}{\partial x_j}|_{x_{ij}^{k}} + \alpha_k . \mathrm{R2} . V_{\mathrm{i},j}^{k-1} \quad (16)$$

$$i = 1, \dots, NP\ k = 1, \dots, k_{\max},$$

Now α_k indicates the rate of inertia or momentum coefficients, and $R2$ indicates an arbitrary integer within [0,1]. The ratio of the maximal to the minimum velocity of the shark is constrained. The velocity controller is applied to all the stages of SSO:

$$\left|V_{ij}^{k}\right| = \min\left[\left|\eta_k . R1 . \frac{\partial(\mathrm{OF})}{\partial x_j}|_{x_{ij}^{k}} + a_k . R2 . V_{i,j}^{k-1}\right|, \left|\beta_k . V_{ij}^{k-1}\right|\right], \quad (17)$$

$$i = 1, \dots, NP, j = 1, \dots, ND, k = 1, \dots, k_{\max}$$

Whereas β_k = velocity limiter ratio for stage k. Due to the forward movement of the shark, its novel position Y_i^{k+1} is determined based on previous velocity and position:

$$Y_i^{k+1} = X_i^{k} + V_i^{k} . \Delta t_k\ i = 1, \dots, NP\ k = 1, \dots, k_{\max} \quad (18)$$

Where Δt_k = time interval of stage k. Δt_k considers 1 to all the stages for the purpose of simplicity.

All the components of $V_{i,j}^{k} (j = 1, \dots, ND)$ of vector V_i^{k} are obtained using Eq. (17). From the optimization, to identify a solution, the shark safeguards a local search in all the stages. This local search in the SSO approach is given below:

$$Z_i^{k+1,m} = Y_i^{k+1} + R3 . Y_i^{k+1}\ m = 1, \dots, M\ i = 1, \dots, NP\ k = 1, \dots, k_{\max}, \quad (19)$$

In Eq. (19), $Z_i^{k+1,m}$ shows the position of point m in the local search; $R3$ indicates the arbitrary integer within [-1,1], and M specifies the number of points in the local search of all the stages.

Fitness selection is a critical aspect of the SSO system. The solution encoder was utilized to measure the aptitude (goodness) of candidate solutions. At this point, the accuracy value is a critical state employed to plan a fitness function.

$$Fitness = \max(P) \tag{20}$$

$$P = \frac{TP}{TP + FP} \tag{21}$$

From the expression, TP represents the true positive, and FP denotes the false positive value.

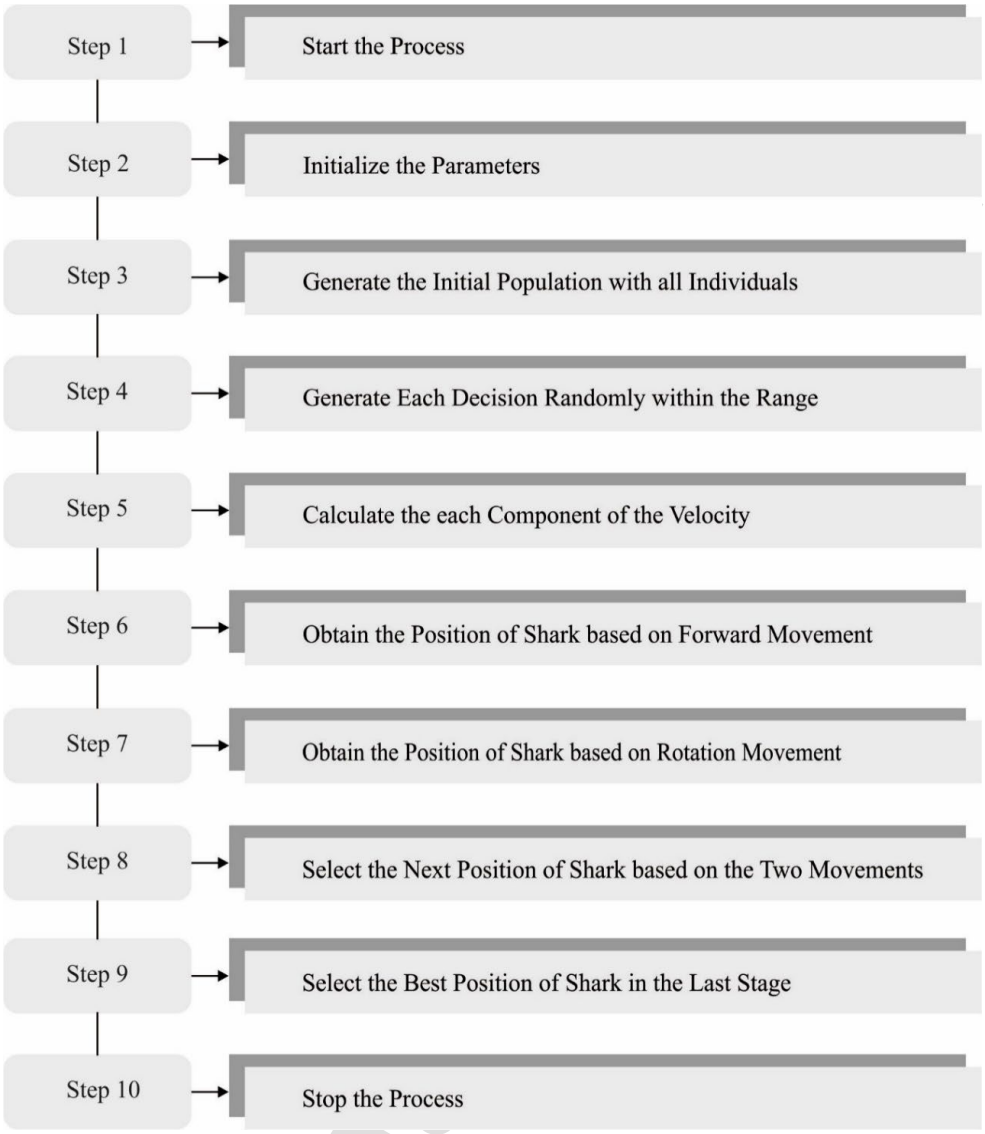

Fig. 2. Steps involved in the SSO technique

3.4. LSTM based Classification

At the final stage, the LSTM-RNN model is employed for the classification of rice seedlings. LSTM-NN is a kind of RNN by adding further memory components [21]. The short-term classifies the data part, the long-term classifies the memory, and the LSTM allocates weight that has the ability to forget or add new data, or the output can be obtained according to the previously stored data of the sample. The LSTM model is particularly well suited to retain and remember input data for a long time and for making essential operations on the memory (write, delete and read).

LSTM configures memory through gated cells and decides either to delete or store the information. The decision has been taken by the gated cells on the basis of the weight coefficient and the change of weight during training. The data with the high impact would be remembered from the LSTM memory in the trained procedure, and the remaining would be removed, which move to achieve the best predicted value. The internal structure of LSTM was intended with three gated cell memory -an input gate to identify and permit the novel input into the model, forget gate to delete the unrelated data, and the resultant gate to determine the ultimate outcome respective to the present state.

LSTM-NN performs backpropagation based GDL and overcomes the occurrence of exploding and vanishing gradients by steep gradient formation with high accuracy of the prediction and minimized training time.

LSTM extends the memory model, and this unit constructs the RNN. In LSTM-NN, data is categorized as short-term, and the memory cell becomes long-term. In this study, the requirement for recurrent LSTM includes:

- To maintain the balanced weight and bias during the training model.
- Unwarranted dismissal of the training process is overcome
- Choose the appropriate activation function to assess the network output
- To improve the memory cell and categorize the data, thus formulate the best testing and training process
- The designed RNN model would be prevented from instability occurrence.
- To pose the best slope value such that the gradient allows an effective train

The steps for training the LSTM network are shown as follows:

Step 1: The network sets a primary weight and another learning parameter. The sigmoid function of the network defines the data which should be obtained forward in a gated cell, and that data must be removed from a given time. The present input x_{t^l} and the preceding state z_{t-1^l} calculate the function and is determined by

$$g_{gt} = \alpha\left(W_{gt.} \bullet \left[z_{(t-1)'} x_t\right] + W_{ogt}\right) \tag{22}$$

Here, $'g_{gt}'$ shows the forget gate, $'\alpha'$ indicates the learning rate metric, $'W_{gt}'$ and $'W_{ogt}'$ defines the weights and bias of the models.

Step 2: it can be essential for adding the memory unit to the present state, and tangent and sigmoid activation function operates to add the memory unit. The operation is given as follows:

$$k_{gt} = \alpha \times \left(W_{it} \bullet \left[z_{(t-1)'} x_t\right] + W_{oit}\right) \tag{23}$$

$$Y_{gt} = \tanh\left(W_{ct} \cdot \left[z_{(t-1)}, x_t\right] + W_{oct}\right) \tag{24}$$

Now, k_{gt} denotes the input gate, and Y_{gt} allocates weight to data by applying the sigmoid function.

Step 3: In this step, the memory cell state where the outcome needs to be obtained is decided. The sigmoid activation layer is to determine the part of the memory cell and the outcome that will calculate the output. Next, the respective cell state takes through the tangent layer to get the value within the interval of $[-1,1]$, and the ultimate outcome from the LSTM-NN model is calculated as follows:

$$R_{gt} = \alpha \times \left(W_{ot} \bullet \left[z_{(t-1)'} x_t\right] + W_{0ot}\right) \tag{25}$$

$$z_t = R_{gt} \times \tanh\left(Y_{gt}\right)$$

Let $'R_{gt}'$ be the output gate which presents the resultant in the memory cells, and $'z_t'$ shows the existing form in which the result was calculated.

4. Experimental Validation

The proposed model is simulated using Python 3.6.5 tool on PC i5-8600k, GeForce 1050Ti 4GB, 16GB RAM, 250GB SSD, and 1TB HDD. The parameter settings are given: learning rate: 0.01, dropout: 0.5, batch size: 5, epoch count: 50, and activation: ReLU.

In this section, the rice seedling classification performance of the SSODL-RSD model is tested using a dataset [22] comprising 20000 samples. The dataset holds 10000 samples under each class, as defined in Table 1. Fig. 3 demonstrates the sample images of bare land and rice seedling.

Table 1 Details of the dataset

Class	**No. of Samples**
Rice Seedling	10000
Bare land	10000

Total Number of Samples	20000

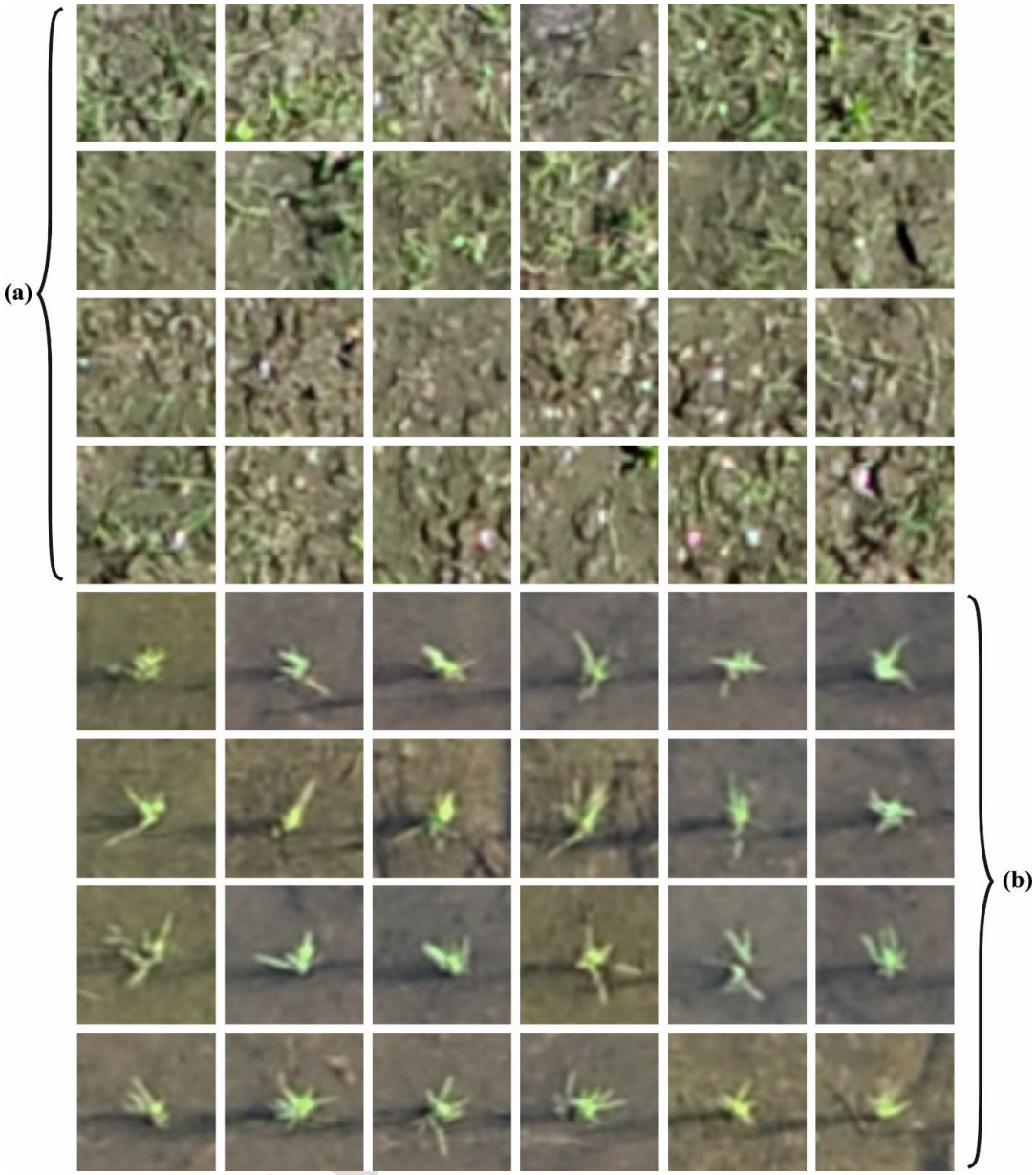

Fig. 3. Sample Images a) Bare Land b) Rice Seedling

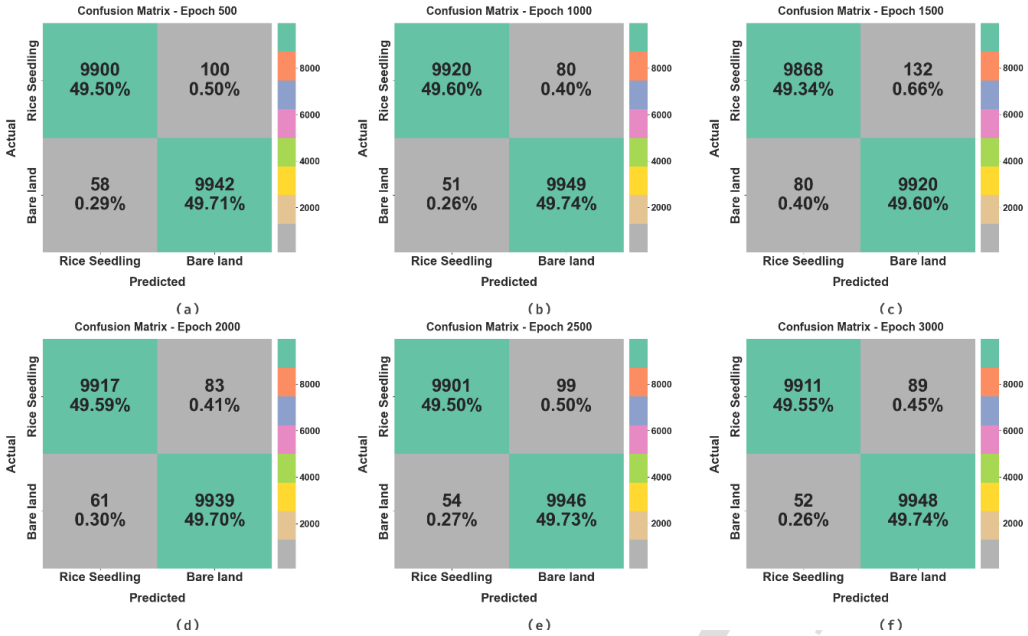

Fig. 4. Confusion matrices of SSODL-RSD approach (a-f) Epoch 500-3000

The rice seedling classification outcomes of the SSODL-RSD model are assessed on distinct epochs in Fig. 4. The results illustrated that the SSODL-RSD model has adequately recognized the input images into rice seedlings and bare land.

Table 2 and Fig. 5 reveal a brief rice seedling classification result of the SSODL-RSD model under several epochs. The experimental outcomes indicated that the SSODL-RSD model has accurately recognized rice seedlings and bare land. For instance, with 500 epochs, the SSODL-RSD model has obtained an average $accu_{bal}$ of 99.21%, $prec_n$ of 99.21%, $reca_l$ of 99.21%, F_{score} of 99.21%, and MCC of 98.42%. Concurrently, with 1000 epochs, the SSODL-RSD approach has reached an average $accu_{bal}$ of 99.34%, $prec_n$ of 99.35%, $reca_l$ of 99.34%, F_{score} of 99.34%, and MCC of 98.69%. Simultaneously, with 1000 epochs, the SSODL-RSD system has gained an average $accu_{bal}$ of 99.28%, $prec_n$ of 99.28%, $reca_l$ of 99.28%, F_{score} of 99.28%, and MCC of 98.56%. Finally, with 1000 epochs, the SSODL-RSD methodology has acquired an average $accu_{bal}$ of 99.29%, $prec_n$ of 99.30%, $reca_l$ of 99.29%, F_{score} of 99.29%, and MCC of 98.59%.

Table 2 Rice seedling classifier outcome of SSODL-RSD system with varying epochs

Class Labels	$Accuracy_{bal}$	Precision	Recall	F-Score	MCC
Epoch-500					
Rice Seedling	99.00	99.42	99.00	99.21	98.42

Bare land	99.42	99.00	99.42	99.21	98.42
Average	**99.21**	**99.21**	**99.21**	**99.21**	**98.42**
Epoch-1000					
Rice Seedling	99.20	99.49	99.20	99.34	98.69
Bare land	99.49	99.20	99.49	99.35	98.69
Average	**99.34**	**99.35**	**99.34**	**99.34**	**98.69**
Epoch-1500					
Rice Seedling	98.68	99.20	98.68	98.94	97.88
Bare land	99.20	98.69	99.20	98.94	97.88
Average	**98.94**	**98.94**	**98.94**	**98.94**	**97.88**
Epoch-2000					
Rice Seedling	99.17	99.39	99.17	99.28	98.56
Bare land	99.39	99.17	99.39	99.28	98.56
Average	**99.28**	**99.28**	**99.28**	**99.28**	**98.56**
Epoch-2500					
Rice Seedling	99.01	99.46	99.01	99.23	98.47
Bare land	99.46	99.01	99.46	99.24	98.47
Average	**99.24**	**99.24**	**99.24**	**99.23**	**98.47**
Epoch-3000					
Rice Seedling	99.11	99.48	99.11	99.29	98.59
Bare land	99.48	99.11	99.48	99.30	98.59
Average	**99.29**	**99.30**	**99.29**	**99.29**	**98.59**

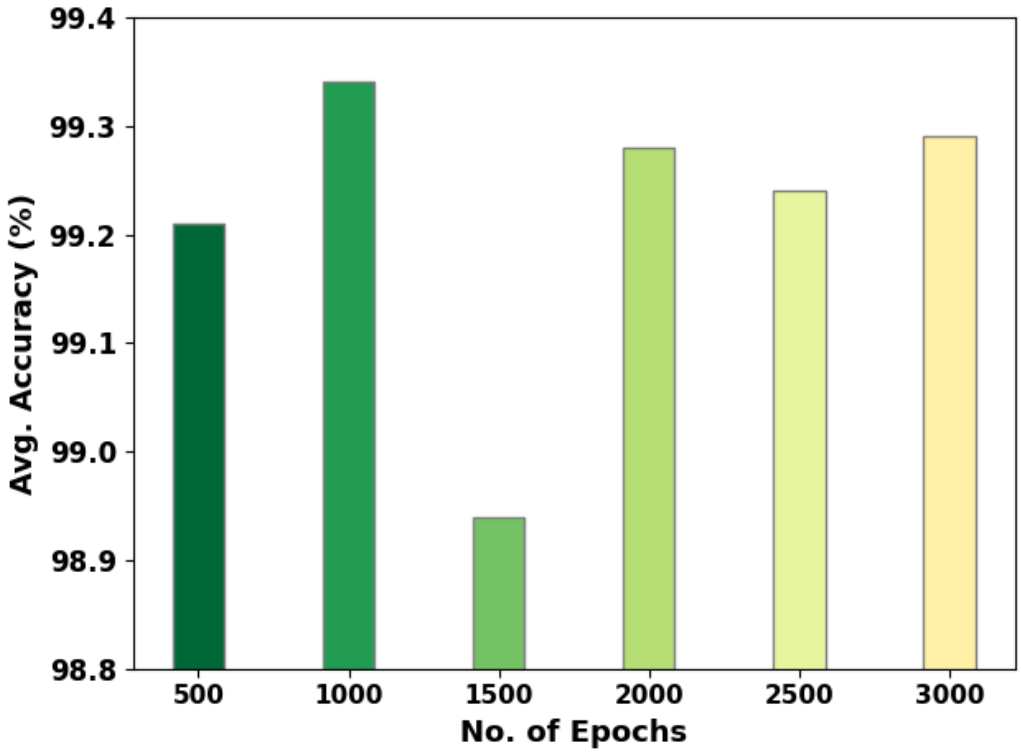

Fig. 5. Average outcome of SSODL-RSD algorithm with varying epochs

The TACC and VACC of the SSODL-RSD approach are investigated on rice seedling performance in Fig. 6. The figure demonstrated that the SSODL-RSD algorithm had exposed enhanced performance with higher values of TACC and VACC. It is evident that the SSODL-RSD system has reached maximal TACC outcomes.

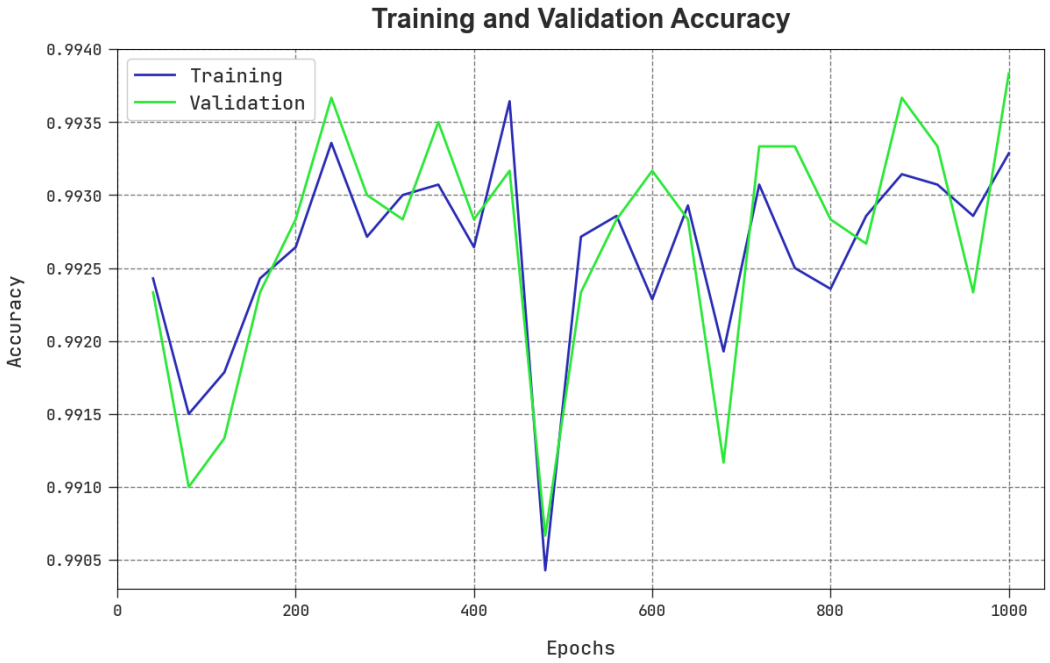

Fig. 6. TACC and VACC outcome of SSODL-RSD algorithm

Fig. 7. TLS and VLS outcome of SSODL-RSD algorithm

The TLS and VLS of the SSODL-RSD methodology are tested on rice seedling performance in Fig. 7. The figure implied that the SSODL-RSD approach had exposed superior performance with minimal values of TLS and VLS. It is observable that the SSODL-RSD method has resulted in reduced VLS outcomes.

An evident precision-recall study of the SSODL-RSD algorithm in the test database is represented in Fig. 8. The figure pointed out that the SSODL-RSD system has led to higher values of precision-recall values in two classes.

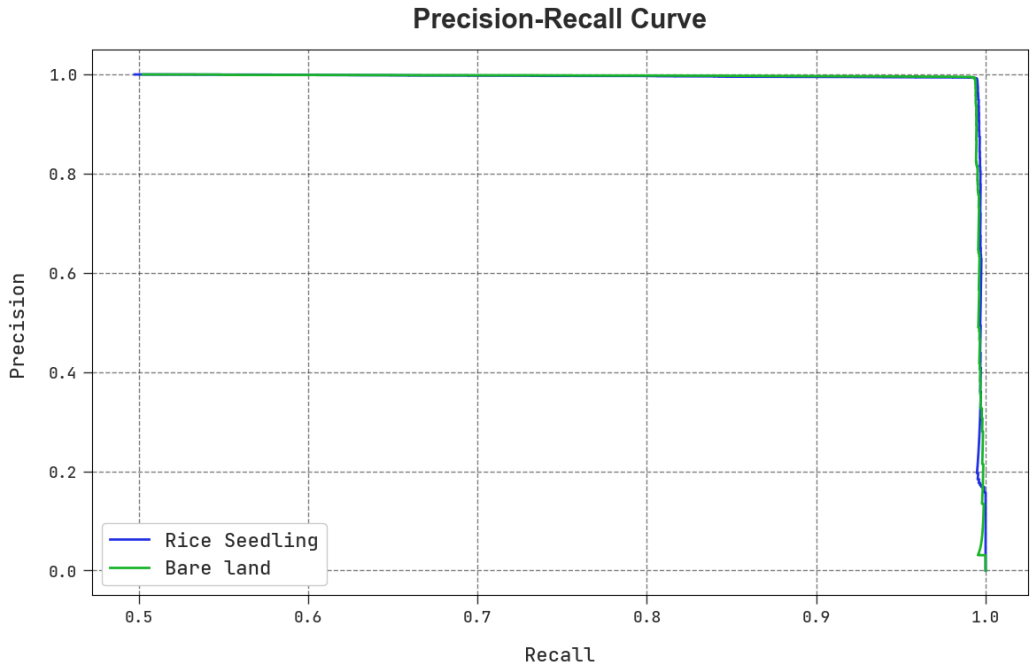

Fig. 8. Precision-recall outcome of SSODL-RSD algorithm

To reassure the improved results of the SSODL-RSD model on rice seedling classification, a wide-ranging comparison study is made in Table 3 [12, 13]. Fig. 9 demonstrates a comparative $accu_y$ examination of the SSODL-RSD approach with other DL techniques. The results indicated that the SSODL-RSD system had shown improved performance over existing ones. Based on $accu_y$, the SSODL-RSD technique has reached an increased $accu_y$ of 99.34%, whereas the EfficientDet, Faster RCNN, HOG-SVM, EfficientNet, and ResNetv2-LSTM models have obtained reduced $accu_y$ of 95.47%, 97.28%, 98.55, 98.10%, and 96.14% respectively.

Table 3 Comparative outcome of SSODL-RSD approach with other DL techniques

Methods	Accuracy	Precision	Recall	F-Score
SSODL-RSD	99.34	99.35	99.34	99.34
EfficientDet	95.47	95.73	95.59	97.60
Faster R-CNN	97.28	96.62	96.44	96.72
HOG-SVM	98.55	96.32	97.86	98.13
EfficientNet	98.10	97.09	96.52	98.46
ResNetv2-LSTM	96.14	96.16	96.92	95.51

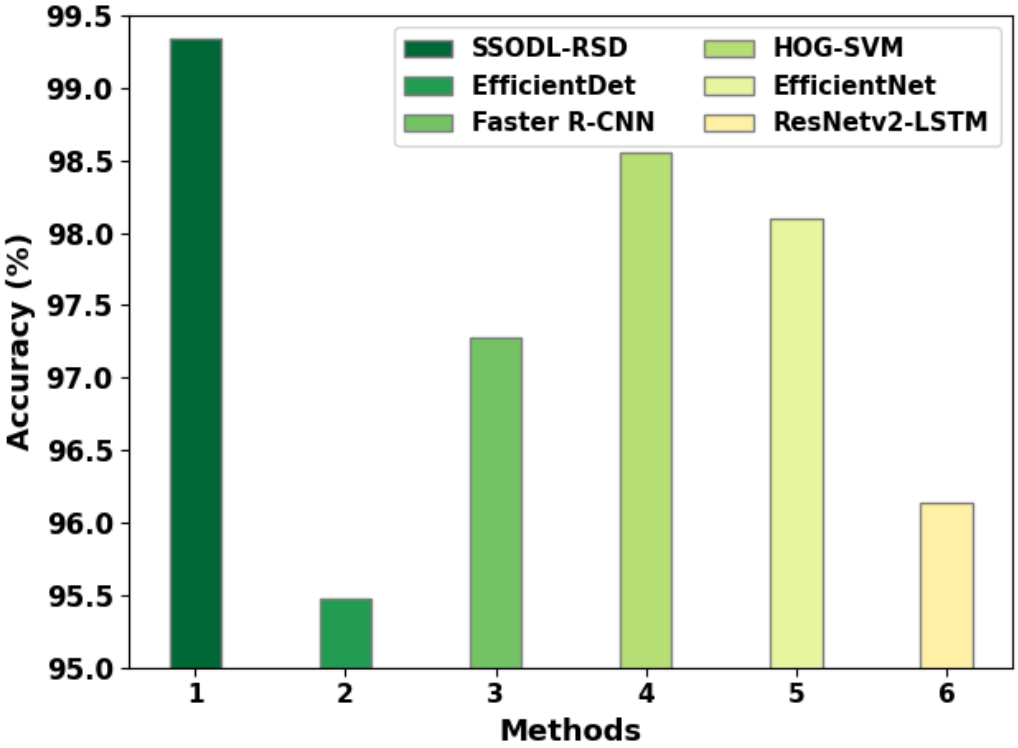

Fig. 9. $Accu_y$ outcome of SSODL-RSD approach with other DL techniques

Fig. 10 determines a comparative $prec_n$, $reca_l$ and F_{score} investigation of the SSODL-RSD approach with other DL techniques. The outcomes exposed that the SSODL-RSD system has shown improved performance over existing ones. With respect to $prec_n$, the SSODL-RSD technique has gained an enhanced $prec_n$ of 99.35%, whereas the EfficientDet, Faster RCNN, HOG-SVM, EfficientNet, and ResNetv2-LSTM approaches have obtained reduced $prec_n$ of 95.73%, 96.62%, 96.32%, 97.09% and 96.16% correspondingly. In the meantime, interms of $reca_l$, the SSODL-RSD approach has reached an increased $reca_l$ of 99.34%% whereas the

EfficientDet, Faster RCNN, HOG-SVM, EfficientNet, and ResNetv2-LSTM systems have acquired decreased $reca_l$ of 95.59%, 96.44%, 97.86%, 96.52% and 96.92%. Finally, based on F_{score}, the SSODL-RSD system has gained an improved $reca_l$ of 99.34%, whereas the EfficientDet, Faster RCNN, HOG-SVM, EfficientNet, and ResNetv2-LSTM systems have attained minimal F_{score} of 97.60%, 96.72%, 98.13%, 98.46% and 95.51%.

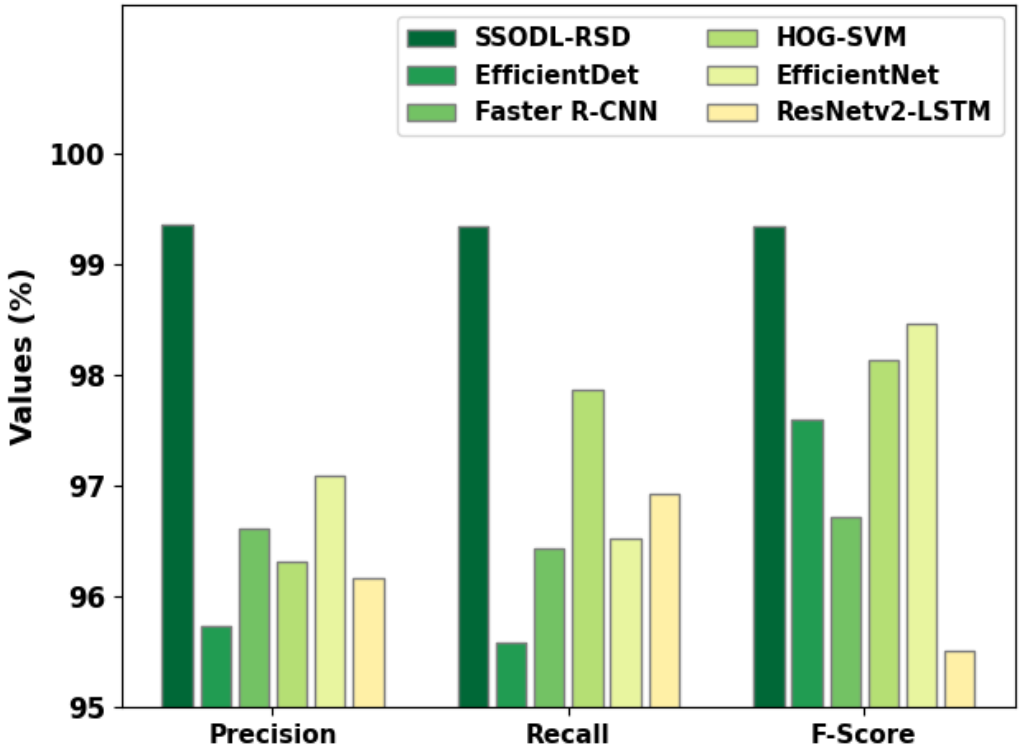

Fig. 10. Comparative outcome of SSODL-RSD approach with other DL techniques

These results signified the improved performance of the SSODL-RSD approach over other existing techniques on rice seedling classification.

5. Conclusion

In this study, we have concentrated on developing the SSODL-RSD technique for rice seedling classification on UAV imagery. The SSODL-RSD technique properly recognized the UAV images into arable land and rice seedlings. Primarily, the SSODL-RSD technique employed the AWF technique for the noise removal procedure. In addition, the SSODL-RSD technique exploited the NestNet feature extractor model. Moreover, the SSO algorithm is used for the hyperparameter tuning of the NestNet model. Finally, the LSTM-RNN model is employed for

the classification of rice seedlings. The experimental evaluation of the SSODL-RSD technique is tested on a rice seedling dataset. The extensive comparative study highlighted the improved outcomes of the SSODL-RSD technique over other existing models. Thus, the SSODL-RSD technique finds useful for accurate rice seedling classification. In future, the performance of the SSODL-RSD technique can be boosted by the multi-modal rice seedling classification technique.

Acknowledgment

The authors are thankful to Deanship of Scientific Research and under the supervision of the Science and Engineering Research Center at Najran University for funding this work under the Research Centers Funding program with grant code (NU/RCP/SERC/12/18).

Conflict of Interest

The authors declare that they have no conflict of interest. The manuscript was written through the contributions of all authors. All authors have given approval for the final version of the manuscript.

Data Availability Statement

Data sharing is not applicable to this article as no datasets were generated during the current study.

Ethics approval

This article does not contain any studies with human participants performed by any of the authors.

Consent to Participate

Not applicable.

Informed Consent

Not applicable.

References

[1] Gilanie, G., Nasir, N., Bajwa, U.I. and Ullah, H., 2021. RiceNet: convolutional neural networks-based model to classify Pakistani grown rice seed types. *Multimedia Systems*, *27*(5), pp.867-875.

[2] Yang, Q., Shi, L., Han, J., Yu, J. and Huang, K., 2020. A near real-time deep learning approach for detecting rice phenology based on UAV images. *Agricultural and Forest Meteorology*, *287*, p.107938.

[3] Margapuri, V., Penumajji, N. and Neilsen, M., 2021, December. Seed Classification using Synthetic Image Datasets Generated from Low-Altitude UAV Imagery. In *2021 20th IEEE International Conference on Machine Learning and Applications (ICMLA)* (pp. 116-121). IEEE.

[4] Dilmurat, K., Sagan, V., Maimaitijiang, M., Moose, S. and Fritschi, F.B., 2022. Estimating Crop Seed Composition Using Machine Learning from Multisensory UAV Data. *Remote Sensing*, *14*(19), p.4786.

[5] Kumar, R., Baloch, G., Buriro, A.B. and Bhatti, J., 2021. Fungal blast disease detection in rice seed using machine learning. *International Journal of Advanced Computer Science and Applications*, *12*(2).

[6] Conrad, A.O., Li, W., Lee, D.Y., Wang, G.L., Rodriguez-Saona, L. and Bonello, P., 2020. Machine learning-based presymptomatic detection of rice sheath blight using spectral profiles. *Plant Phenomics*, *2020*.

[7] Tan, S., Liu, J., Lu, H., Lan, M., Yu, J., Liao, G., Wang, Y., Li, Z., Qi, L. and Ma, X., 2022. Machine Learning Approaches for Rice Seedling Growth Stages Detection. *Frontiers in Plant Science*, *13*.

[8] Liao, F., Feng, X., Li, Z., Wang, D., Xu, C., Chu, G., Ma, H., Yao, Q. and Chen, S., A Spatio-Temporal Conval Neural Network Model for Rice Nutrient Level Diagnosis at Rice Panicle Initiation Stage. *Available at SSRN 4272680*.

[9] Muharam, F.M., Nurulhuda, K., Zulkafli, Z., Tarmizi, M.A., Abdullah, A.N.H., Che Hashim, M.F., Mohd Zad, S.N., Radhwane, D. and Ismail, M.R., 2021. UAV-and Random-Forest-AdaBoost (RFA)-based estimation of rice plant traits. *Agronomy*, *11*(5), p.915.

[10] Yamaguchi, T., Tanaka, Y., Imachi, Y., Yamashita, M. and Katsura, K., 2020. Feasibility of combining deep learning and RGB images obtained by unmanned aerial vehicle for leaf area index estimation in Rice. *Remote Sensing*, *13*(1), p.84.

[11] Anuar, M.M., Halin, A.A., Perumal, T. and Kalantar, B., 2022. Aerial imagery paddy seedlings inspection using deep learning. *Remote Sensing*, *14*(2), p.274.

[12] Tseng, H.H., Yang, M.D., Saminathan, R., Hsu, Y.C., Yang, C.Y. and Wu, D.H., 2022. Rice seedling detection in UAV images using transfer learning and machine learning. *Remote Sensing*, *14*(12), p.2837.

[13] Yang, M.D., Tseng, H.H., Hsu, Y.C., Yang, C.Y., Lai, M.H. and Wu, D.H., 2021. A UAV open dataset of rice paddies for deep learning practice. *Remote Sensing*, *13*(7), p.1358.

[14] Wu, J., Yang, G., Yang, X., Xu, B., Han, L. and Zhu, Y., 2019. Automatic counting of in situ rice seedlings from UAV images based on a deep fully convolutional neural network. *Remote Sensing*, *11*(6), p.691.

[15] Wang, S., Zhang, W., Wang, X. and Yu, S., 2021. Recognition of rice seedling rows based on row vector grid classification. *Computers and Electronics in Agriculture*, *190*, p.106454.

[16] Nguyen-Quoc, H. and Hoang, V.T., 2020. Rice seed image classification based on HOG descriptor with missing values imputation. *TELKOMNIKA (Telecommunication Computing Electronics and Control)*, *18*(4), pp.1897-1903.

[17] Ma, X., Deng, X., Qi, L., Jiang, Y., Li, H., Wang, Y. and Xing, X., 2019. Fully convolutional network for rice seedling and weed image segmentation at the seedling stage in paddy fields. *PloS one*, *14*(4), p.e0215676.

[18] Nirmalapriya, G., Agalya, V., Regunathan, R. and Ananth, M.B.J., 2023. Fractional Aquila spider monkey optimization based deep learning network for classification of brain tumor. *Biomedical Signal Processing and Control*, *79*, p.104017.

[19] Yu, X., Fan, J., Chen, J., Zhang, P., Zhou, Y. and Han, L., 2021. NestNet: A multiscale convolutional neural network for remote sensing image change detection. *International Journal of Remote Sensing*, *42*(13), pp.4898-4921.

[20] Manjunath, K., Ramaiah, G.K. and GiriPrasad, M.N., 2022. Backward movement oriented shark smell optimization-based audio steganography using encryption and compression strategies. *Digital Signal Processing*, *122*, p.103335.

[21] Shanmuganathan, J., Victoire, A.A., Balraj, G. and Victoire, A., 2022. Deep Learning LSTM Recurrent Neural Network Model for Prediction of Electric Vehicle Charging Demand. *Sustainability*, *14*(16), p.10207.

[22] https://github.com/aipal-nchu/RiceSeedlingDataset

Yousef A. Asiri is an Assistant Professor in the Department of Computer Science, College of Computer Science and Information Systems in Najran University. Yousef is a research member in the Scientific and Engineering Research Center (CERC) at Najran University. Yousef has many publications in different impact factor journals. Yousef's main interest is to study how computers affect human lives in various aspect such as health, education, psychology and environment. Yousef is also in general interested in the area of Human-computer Interaction and Design using machine learning, deep learning, data mining techniques and intelligent systems.

Unmanned Aerial Vehicles Assisted Rice Seedling Detection using Shark Smell Optimization with Deep Learning Model

Authors Statement

Conceptualization, Data curation and Formal analysis, Investigation and Methodology, Writing —original draft, Validation and Visualization: Yousef A. Asiri

Unmanned Aerial Vehicles Assisted Rice Seedling Detection using Shark Smell Optimization with Deep Learning Model

Declaration of interests

- The authors declare that they have no known competing financial interestsor personal relationships that could have appeared to influence the work reported in this paper.

- The authors declare the following financial interests/personal relationships which may be considered as potential competing interests:

- All authors have participated in (a) conception and design, or analysis and interpretation of the data; (b) drafting the article or revising it critically for important intellectual content; and (c) approval of the final version.

- This manuscript has not been submitted to, nor is under review at, another journal or other publishing venue.

Sincerely,

Yousef Asiri

Corresponding author

(on behalf of all the authors)